Photoionization time-of-flight mass spectrometry studies on iron pentacarbonyl-doped hydrogen/oxygen flat flames

S. Kluge*[1], T. Bierkandt[1], I. Wlokas[1, 2], T. Kasper[1, 2], H. Wiggers[1, 2], C. Schulz[1, 2]

[1]IVG, Institute for Combustion and Gas Dynamics, University of Duisburg-Essen, 47048 Duisburg, Germany

[2]CENIDE, Center for Nanointegration Duisburg-Essen, 47048 Duisburg, Germany

Abstract

Nanoparticle synthesis in low-pressure flat flames is studied by means of photoionization time-of-flight mass spectrometry (PI-TOF-MS). We present results of energy scans representing photoionization efficiency curves of $Fe(CO)_5$ as well as burner scans of an undoped and a doped H_2/O_2 flames that give insight into the flame chemistry. The concentration profiles of decomposition products of $Fe(CO)_5$ and other flame species are compared to the results of chemical kinetics modeling according to the mechanism proposed by Feroughi et al. [Proc. Combust. Inst. 35 (2015) 2299-2306].

Introduction

Molecular-beam mass spectrometry methods enable the inline investigation of the gas-phase synthesis of nanoparticles in flames. Molecular-beam sampling from a reacting flow suddenly interrupts all reactions in the gas sample and thus allows determining a gas-phase and particle-phase composition that is representative for the gas composition in the reactor. Gas phase molecules in the beam are detected according to their mass-to-charge ratios (m/z) in a time-of-flight mass spectrometer (TOF-MS). The measurements yield the gas-phase composition at various locations in the reactor. The aim of our study is to observe the influence of the addition of iron pentacarbonyl $Fe(CO)_5$ on the flame chemistry of a H_2/O_2 flame and the precursor decomposition and the initial particle formation by the use of synchrotron photoionization (PI) time-of-flight mass spectrometry.

Iron oxide nanoparticles are synthesized through the decomposition of iron pentacarbonyl $Fe(CO)_5$ in a premixed H_2/O_2 flame. An almost one-dimensional, low-pressure flat flame operated at 33.3 mbar is used to spatially extend the reaction zone. At various locations downstream of the burner head, small samples of the aerosol are expanded through a nozzle and a skimmer into high-vacuum to form a particle-laden molecular beam. The decomposition of the precursor and its influence on flame chemistry can be studied by varying the distance between the burner head relative to the nozzle position ("burner scan") which represents the residence time within the reactor.

For mass spectrometry the species of interest must be ionized. The widely used electron impact ionization (EI) has the drawback that the energy distribution of the electrons is comparatively broad. Additionally, ionization with high-kinetic-energy electrons can lead to fragmentation during the ionization process. In contrast, single photon photoionization (SPI) uses vacuum ultraviolet (VUV) photons generated by the beamline of a synchrotron. A monochromator tunes the photon energy precisely ("energy scan") which allows distinguishing between molecules with the same mass but different ionization thresholds. In addition, the fragmentation of fragile intermediate species is reduced. Both effects together dramatically increase the quality of information that can be gained from mass spectrometry using SPI by synchrotron light as reviewed from Hansen et al. [1]. We present results of energy scans representing photoionization efficiency curves of $Fe(CO)_5$ as well as burner scans of undoped and a doped H_2/O_2 flames that give insight into the flame chemistry. The concentration profiles of decomposition products of $Fe(CO)_5$ and other flame species are compared to the results of chemical kinetics modeling according to the mechanism proposed by Feroughi et al. [2].

Experiment

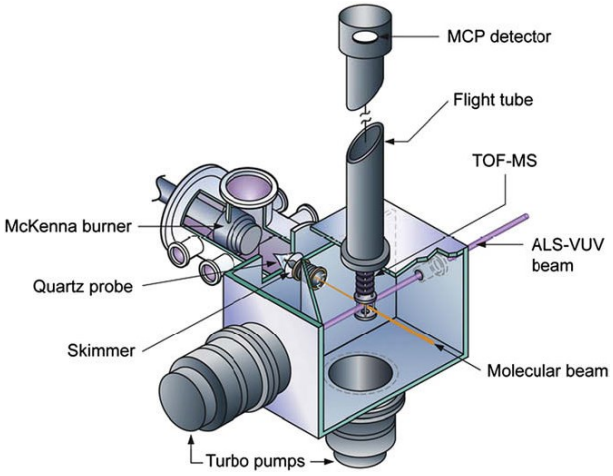

Figure 1: Experimental setup [1]

The synchrotron photoionization (PI) time-of-flight mass spectrometer shown in Figure 1 is described in detail in [1, 3]. It is located at the chemical kinetics

* Corresponding author: sebastian.kluge@uni-due.de

beamline of the Advanced Light Source (ALS), Berkeley, USA. A low-pressure flat-flame of 1 slm H_2 and 1 slm O_2 diluted by 2 slm Ar is stabilized on a McKenna burner at 33.3 mbar. A molecular beam is formed by expanding the flame gases through a 80 µm quartz probe and a 2 mm skimmer located 23 mm downstream of the probe. The pressure in the two expansion stages are 10^{-4} mbar and 10^{-6} mbar, respectively. The molecular beam is ionized by the VUV beam that can be tuned precisely over the 7.8–17 eV range [3].

Simulation

Simulations of the undoped and the doped flame are performed with a mechanism based on the scheme presented recently by Feroughi et al. [2] for $Fe(CO)_5$ doped CH_4/O_2 diffusion flames. The iron oxide formation sub-mechanism was based on the work of Wlokas et al. [4], while the iron cluster formation was taken from the mechanism by Wen et al. [5]. For simulations of the H_2/O_2 flame, the sub-mechanism of $Fe(CO)_5$ flame interaction was combined with the C1-Mechanism by Li et al. [6]. The simulations were performed for the measured temperature profiles as one-dimensional flames, using the open source kinetics software Cantera [7].

Data evaluation strategy

Data evaluation according to the procedure described by Schenk et al. [8] consists of several steps. Each peak was automatically fitted by a Gaussian profile. The area of the fit was plotted either against the height of the burner (HAB, burner scan) or the energy of the photons (energy scan).

Using a cold gas flow of a commercial mixture with a known composition of gaseous components (hydrogen, methane, acetylene, carbon monoxide, carbon dioxide, krypton, xenon, argon) one can derive both a calibration for the conversion between time-of-flight and respective mass and the mass discrimination factor of the setup.

The mass discrimination factor accounts for the depletion of light mass compared to heavier components due to pressure diffusion and Mach-number focusing during the formation of the molecular beam. Pressure diffusion describes greater divergence of lighter species from the beam axis due to radial pressure gradients in the continuum regime of the sampling cone. Mach-number focusing takes place in the free-molecular regime between the sampling cone and the skimmer where the transversal thermal velocity component of the species is superimposed on the directed downstream velocity. It causes lighter species to be more deflected from the central axis because the thermal velocity is inversely proportional to the square root of the mass. Combining both effects the concentration of lighter species is reduced on the centerline of the molecular beam where ionization takes place [3].

Flame reactions produce species with the same mass-to-charge ratios as fragmentation processes due to the ionization of molecules with excess energy in the ionization region of the instrument (photofragmentation). To account for the influence of photofragmentation an energy of the photon below the fragmentation energy of the parent ion was used if possible. For iron pentacarbonyl $Fe(CO)_5$ and its fragments an energy above the fragmentation threshold has to be used due to lack of sensitivity. Therefore, the measured fragmentation probability of $Fe(CO)_5$ has been taken into account in the analysis of the profiles of the fragment ions.

The photoionization cross sections of commonly used components like H_2 [9, 10], O_2 [11], Ar [12], H_2O [13], Kr [12], Xe [12], CH_4 [14], C_2H_2 [15], CO [16], CO_2 [17] and well-studied intermediates (O [18], OH [19]) are taken from the literature. They are needed to quantify the mass signals.

The temperature profiles of the flames have been calculated from the Ar signal according to:

$$T_x = \frac{\overline{M_x}\, S_x^2\, x_1^2}{\overline{M_1}\, x_x^2\, S_1^2}\, T_1 \qquad (1)$$

with:
index x: given position
index 1: reference position in the exhaust gas
$\overline{M_{x,1}}$ mean molar mass
$S_{x,1}$ argon signal
$x_{x,1}$ mole fraction of argon
T_1 temperature at the reference position

Results

A photoionization spectrum of $Fe(CO)_5$ is shown in Figure 2. From linear interpolation of the ion signals near their respective onsets appearance energies can be determined. The results are listed in Table 1 together with literature values from TEPICO [20] experiments on cold beams of $Fe(CO)_5$ or residual (thermal) $Fe(CO)_5$, PEPICO [21] and sector mass spectrometer measurements [22].

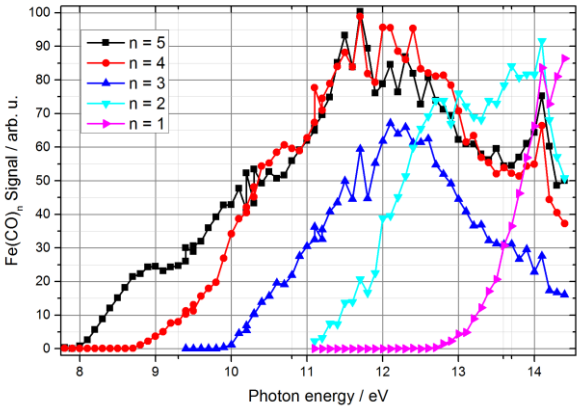

Figure 2: Photoionization spectrum of $Fe(CO)_5$

The ionization energy of iron pentacarbonyl is 8 eV. At higher photon energies photofragmentation takes place starting with $FeCO_4$ as a fragment at 8.8 eV. Vertical lines inside the graph indicate the energies used

for burner scans. At 10.8 eV for example the signal TOF-MS signals of $Fe(CO)_5$ and $Fe(CO)_4$ are equal due to the fragmentation probability if no $Fe(CO)_4$ is present in the flame. As already discussed above subtraction of the photofragmentation related signal is needed to calculate a profile for $Fe(CO)_4$ at 10.8 eV ionization energy. All the appearance energies are in good agreement to the literature values.

Table 1: Appearance energy of different fragments

Ion	Appearance energy / eV				
	This work	[22]	[21]	[20] thermal	[20] cold
$Fe(CO)_5^+$	8.0	7.98	7.897		
$Fe(CO)_4^+$	8.8	8.77	8.670	8.86	9.20
$Fe(CO)_3^+$	10.0	9.72	9.763	9.69	10.17
$Fe(CO)_2^+$	11.1	10.70	10.876	10.88	11.27
$Fe(CO)_1^+$	12.7	11.53	12.677	12.40	12.40
Fe^+		14.03	14.383	14.59	14.58

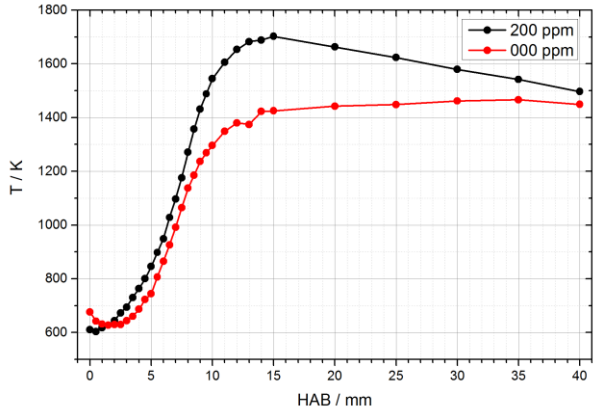

Figure 3: Temperature profiles of the flames

The temperature profiles of the undoped and the doped flame are shown in Figure 3. The temperature close to the burner surface is between 600 and 700 K for both flames followed by a sharp increase in temperature as the height above the burner (HAB) increases. The maximum temperature is around 1500 K for the undoped flame. Doping the flame with 200 ppm $Fe(CO)_5$ increases the maximum temperature to 1700 K. The exhaust gas temperature was measured to be around 1500 K in both cases.

Main species profiles for the undoped (solid lines) and the doped (dotted lines) flames are shown in Figure 4. The profiles of the stable components Ar, H_2, O_2 and H_2O are nearly the same for both flames. As expected the mole fraction of argon does not change a lot as argon is inert and the total number of gaseous moles stays nearly the same (−12.5 mol) according to the net reaction equation 2:

$$H_2 + O_2 + 2\ Ar \rightarrow H_2O + 0.5\ O_2 + 2\ Ar \qquad (2)$$

H_2 as the fuel is consumed within the first 10 mm in good agreement to the O_2 concentration profile that reaches its final value also around 10 mm HAB. At 10 mm HAB the final mole fraction of the only product H_2O is also reached indicating a complete reaction within the first 10 mm of the undoped flame.

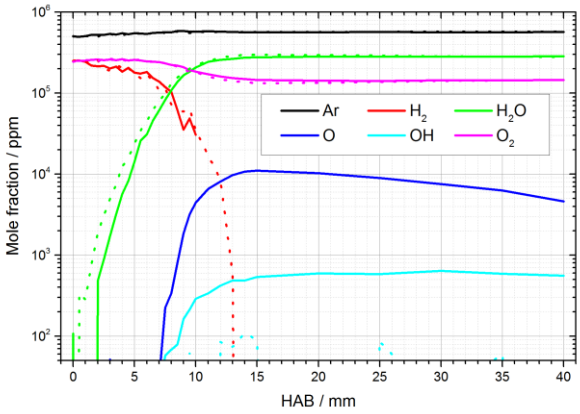

Figure 4: Main species profiles (solid lines undoped, dotted lines doped flame)

The main difference between the undoped and the doped flame (200 ppm $Fe(CO)_5$) is that the mole fractions of the O and OH radicals in the doped flame are below the detection limit indicating reactions with iron containing species acting as a sink for the flame radicals.

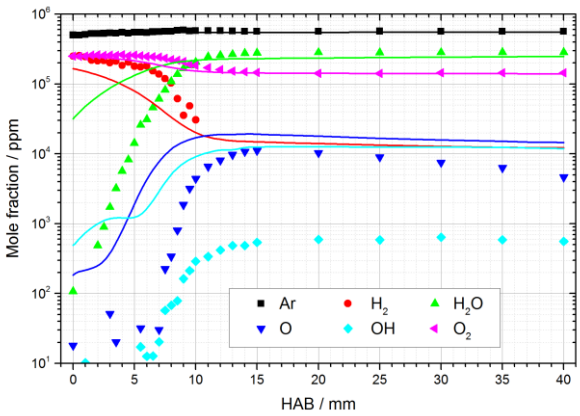

Figure 5: Main species of the undoped flame compared to the model calculations

Figure 5 shows the results of a simulation using the mechanism published by Feroughi et al. [2] and the temperature profile shown in Figure 3 for the undoped flame. The qualitative agreement between the measured and the simulated profiles is acceptable. The measured profiles seem to be shifted towards larger HAB by around 3 mm. This may be explained by the effect of sampling from a finite volume in front of the nozzle which changes the profiles especially in the presence of high concentration gradients inside the flame front [1].

The same effect of a shifted profile can be seen by comparing the main species profiles measured by TOF-MS with the simulation results for the doped flame as can be seen in Figure 6.

Even though the model predicts a smaller amount of oxygen radicals compared to the undoped flame it does not explain that there is no more oxygen radical related

TOF-MS signal left. The reason for this observation is likely related to the sample extraction from the flame. The sensitivity of the instrument for reactive O and OH radicals is limited because these radicals seem to recombine or react with the walls of the nozzle and prevents the detection of O radicals in the doped flame. The unaccountable sampling losses are often compensated in the data analysis by determining the radical mole fractions of O, H and OH from partial equilibrium calculations in the exhaust gas [23] rather than the use of uncertain ionization cross sections. However, given that the effect of the iron containing species on the reactions in the recombination zone of the flame is not as well characterized as the equilibrating reactions in neat hydrogen flames this procedure is not applicable here.

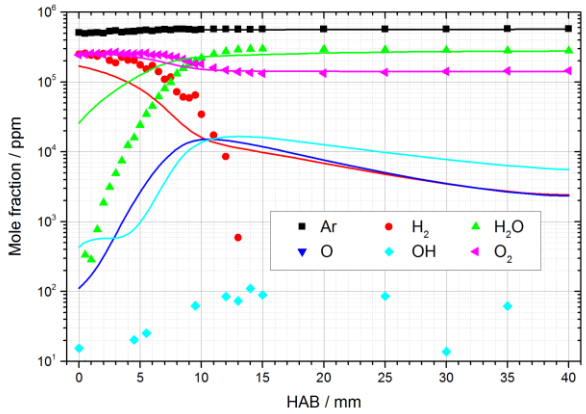

Figure 6: Mole fractions of the main species in the $Fe(CO)_5$ doped flame

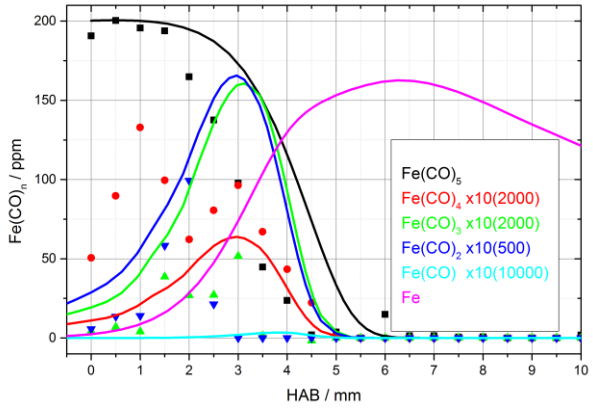

Figure 7: Species concentration profiles for $Fe(CO)_n$

The mole fraction profiles of iron pentacarbonyl and its fragments are plotted in Figure 7. The measured fragment profiles are corrected for photofragmentation and amplified by a factor of 10 for better visibility. The simulated profiles of the fragments were also amplified for $Fe(CO)_4$ and $Fe(CO)_3$ by a factor of 2000, for $Fe(CO)_2$ by 500 and for $Fe(CO)_1$ by 10000. Symbols represent the measured data while the lines are simulation results. Unlike the main species concentration profiles in Figure 5 and Figure 6 the measured signal of $Fe(CO)_5$ seems to be shifted by 1.25 mm to lower heights above burner. One explanation could be that iron pentacarbonyl already decomposes in the burner. However, the burner is water-cooled and its temperature does not exceed 100°C. Another explanation could be that the reaction rates for the initial decomposition step do not capture the reactions in the flame correctly. Species profiles of these decomposition products have not been available for model development previously.

$Fe(CO)_4$ as the main fragment has a maximum mole fraction of 13 ppm at 1 mm HAB. Later also $Fe(CO)_3$ and $Fe(CO)_2$ can be detected (5 ppm at 3 mm and 10 ppm at 2 mm). The error in the profile calculation for the fragments is rather high. For example, there is a high sensitivity of the system towards changes in the photo-fragmentation probability between cold gas measurement and flame conditions as indicated by Fieber-Erdmann et al. [20]. In addition, the concentration of the intermediates is close to the detection limit of the setup. Using photon energies lower than 11 eV to reduce photofragmentation of $Fe(CO)_5$ is crucial but suffers from smaller photon fluxes at the advanced light source compared to the higher photon energies. Most importantly, the sampling nozzle slowly clogged over the 9 hour duration of the experiment. This fact illustrates one of the greatest challenges in the investigation of particle-laden reacting flows: While typically signal-to-noise ratios can be improved by extensive averaging (limited only by the availability of beam-time at synchrotron light sources), the measurement time in particle-laden flows is restricted by the time it takes for the nozzle to clog. In future work, more advanced sampling techniques or inline cleaning procedures have to be implemented to improve data quality.

Conclusions

Iron oxide nanoparticle synthesis in a low-pressure flat flame is studied by photoionization time-of-flight mass spectrometry (PI-TOF-MS). The photoionization spectrum of iron pentacarbonyl shows appearance energies of $Fe(CO)_n^+$ ions in the range of 8.0 eV for $Fe(CO)_5^+$ to 12.7 eV for $Fe(CO)_1^+$ in good agreement with literature values. The process consists of a step-by-step elimination of CO groups.

The main species concentration profiles of the H_2/O_2 flame with and without doping are compared to simulation results that show a shift of the measured signals to slightly larger heights above burner which may be explained by a sampling effect. Doping the flame reduces the amount of O and OH radicals below the detection limit indicating reactions with iron containing species acting as a sink for the radicals.

The measured mole fraction profiles of iron pentacarbonyl and its fragments are shifted to lower heights above the burner if compared to simulation results. This may be either due to decomposition of $Fe(CO)_5$ within the burner or errors in the reaction rates of the initial decomposition steps as species profiles of the decomposition products were not available before.

Acknowledgements

The authors are grateful to the "ALS flame team", in particular Paul Fugazzi and Nils Hansen, for beam time and technical support.

The Advanced Light Source is supported by the Director, Office of Basic Energy Sciences, Material Science Division, of the U.S. Department of Energy. Work in Duisburg (T.B., T.K.) was supported by the Ministry of Innovation, Science and Research of the German state of North Rhine-Westphalia. S.K., H.W., C.S. and I.W. thank for funding by the German Research Foundation within SCHU 1369/13.

References

1. N. Hansen; T. A. Cool; P. R. Westmoreland; K. Kohse-Höinghaus, Progr. Energy Combust. Sci. 35 (2009) 168-191.
2. O. M. Feroughi; S. Hardt; I. Wlokas; T. Hülser; H. Wiggers; T. Dreier; C. Schulz, Proc. Combust. Inst. 35 (2015) 2299-2306.
3. T. A. Cool; A. McIlroy; F. Qi; P. R. Westmoreland; L. Poisson; D. S. Peterka; M. Ahmed, Rev. Sci. Inst. 76 (2005).
4. I. Wlokas; A. Faccinetto; B. Tribalet; C. Schulz; A. Kempf, Int. J. Chem. Kin. 45 (2013) 487-498.
5. J. Z. Wen; C. F. Goldsmith; R. W. Ashcraft; W. H. Green, J. Phys. Chem. C 111 (2007) 5677-5688.
6. J. Li; Z. Zhao; A. Kazakov; M. Chaos; F. L. Dryer; J. J. Scire, Int. J. Chem. Kin. 39 (2007) 109-136.
7. D. G. Goodwin in: *An Open-Source, Extensible Software Suite for CVD Process Simulation*, ECS Proceedings Volume 2003-08, 2003; F. M. M. Allendorf; F. Teyssandier, (Eds.) The Electrochemical Society: 2003; pp 155-162.
8. M. Schenk; L. Leon; K. Moshammer; P. Oßwald; T. Zeuch; L. Seidel; F. Mauss; K. Kohse-Höinghaus, Combust. Flame 160 (2013) 487-503.
9. C. Backx; G. R. Wight; M. J. V. d. Wiel, J. Phys. B 9 (1976) 315-331.
10. M. Glass-Maujean; S. Klumpp; L. Werner; A. Ehresmann; H. Schmoranzer, J. Chem. Phys. 126 (2007).
11. D. M. P. Holland; D. A. Shaw; S. M. McSweeney; M. A. MacDonald; A. Hopkirk; M. A. Hayes, Chem. Phys. 173 (1993) 315-331.
12. J. A. R. Samson; W. C. Stolte, J. Electron Spectrosc. Rel. Phenomena 123 (2002) 265-276
13. D. H. Katayama; R. E. Huffman; C. L. O'Bryan, The Journal of Chemical Physics 59 (1973) 4309-4319.
14. J. Wang; B. Yang; T. A. Cool; N. Hansen; T. Kasper, Int. J. Mass Spectr. 269 (2008) 210-220.
15. T. A. Cool; J. Wang; K. Nakajima; C. A. Taatjes; A. McLlroy, Int. J. Mass Spectr 247 (2005) 18-27.
16. J. A. R. Samson; J. L. Gardner, J. Electron Spectrosc. Rel. Phenomena 8 (1976) 35-44.
17. D. A. Shaw; D. M. P. Holland; M. A. Hayes; M. A. MacDonald; A. Hopkirk; S. M. McSweeney, Chem. Phys. 198 (1995) 381-396.
18. J. A. R. Samson; P. N. Pareek, Phys. Rev. A 31 (1985) 1470-1476
19. P. M. Dehmer, Chem. Phys. Lett. 110 (1984) 79-84.
20. M. Fieber-Erdmann; E. Holub-Krappe; G. Bröker; G. Dujardin; A. Ding, Int. J. Mass Spectr. Ion Proc. 149–150 (1995) 513-520.
21. K. Norwood; A. Ali; G. D. Flesch; C. Y. Ng, J. Am. Chem. Soc. 112 (1990) 7502-7508.
22. G. Distefano, J. Res. Nat. Bur. Stand. A 74 (1970) 233-239
23. N. Hansen; J. A. Miller; P. R. Westmoreland; T. Kasper; K. Kohse-Höinghaus; J. Wang; T. A. Cool, Combust. Flame 156 (2009) 2153-2164.